Potential energy surface and hopping path for hydrogen in $LaNi_5$

Akinori Tezuka,* Hao Wang,† Hiroshi Ogawa, and Tamio Ikeshoji‡
Research Institute for Computational Sciences (RICS), National Institute of Advanced Industrial Science and Technology (AIST), AIST Tsukuba Central 2, Umezono 1-1-1, Tsukuba, Ibaraki 305-8568, Japan
(Received 17 August 2009; revised manuscript received 29 January 2010; published 26 April 2010)

Hydrogen hopping paths in $LaNi_5H$ solid solution were analyzed via first-principles calculations. Potential energy surfaces were determined for hydrogen on the plane with hydrogen sites 6*m*, 12*o*, and 4*h* and on the plane with hydrogen sites 12*n*, 3*f*, and 6*i*. From the zero-point vibration energy along the hopping path, it was found that hydrogen locations are grouped only at three regions; quasi-*m* site (*o*-*m*-*o*), *h* site, and quasi-*f* site (*i*-*f*-*i*). By applying the nudged elastic band method to hydrogen hopping paths between all the possible two sites, the most probable diffusion route was determined as quasi-*f*–quasi-*m*–quasi-*f* in the ***c*** direction and quasi-*f*–quasi-*m*–quasi-*f*–quasi-*m*–quasi-*f* in the ***a*** and ***b*** directions with the same saddle point energy of 0.37 eV, which is in good agreement with the measured activation energy, 0.3–0.5 eV, of the hydrogen diffusion in the solid solution phase of $LaNi_5$-H system.

DOI: 10.1103/PhysRevB.81.134304 PACS number(s): 61.72.S−, 66.30.−h, 71.15.−m

I. INTRODUCTION

Hydrogen in metals brings various interesting phenomena that are different from those of other atoms. Hydrogen acts like a metal in some metals with no obvious bond formation in a shallow potential. The high diffusion rate and quantum effect of hydrogen nuclei are expected to occur. $LaNi_5$ and its related alloys have been extensively studied as a hydrogen absorption alloy.[1,2] The density of hydrogen in $LaNi_5H_n$ ($n \geq 6$) is much higher than that of liquid hydrogen. $LaNi_5H_n$ can function as a hydrogen storage material because of its large hydrogen storage capacity per volume and its high absorption/desorption rate. The latter property has significant advantage for practical use over the so-called light-metal hydrogen absorption materials, which have, in many cases, low absorption/desorption rates although they show high hydrogen storage capacity per weight.

A hydrogen molecule decomposes into two hydrogen atoms on the surface of the $LaNi_5$ crystal, and then these atoms diffuse into the crystal. The diffusion process with a high rate occurs in the solid solution phase, i.e., for $n<1$ in $LaNi_5H_n$. When n increases, the phase transition to the hydrides, $LaNi_5H_3$ or $LaNi_5H_6$, occurs.[3,4] In the region of $1<n<6$, two phases coexist. The hydrogen absorption/desorption rate in this n region may be related to both the diffusion rate of hydrogen in the solid solution and the movement speed of the phase boundary between the two phases.

Diffusion is experimentally observed as a result of successive hydrogen hopping between neighboring interstitial hydrogen sites. Since, in the case of simple metals such as Ni and Pd, there are only one or two hydrogen sites, the hydrogen atom hops over simple potential energy surfaces. In the case of $LaNi_5H_n$, there are many hydrogen sites that have a complicated potential energy surface. Although experiments determine the diffusion coefficient and its activation energy in the bulk,[5–9] it is difficult to measure each energy barrier of paths between various hydrogen sites. We perform the first-principles calculations to determine hydrogen hopping paths and their relationship to the overall diffusion process.

$LaNi_5$ crystal has a hexagonal structure ($P6/mmm$) whose unit cell is spanned by vectors ***a***, ***b***, and ***c*** ($\|\boldsymbol{a}\|=\|\boldsymbol{b}\|, \boldsymbol{a}\perp\boldsymbol{c}, \boldsymbol{b}\perp\boldsymbol{c}$).[10] Six possible hydrogen sites that are specified by using Wyckoff symbols, i.e., 6*m*, 12*o*, 4*h*, 12*n* (tetragonal), 6*i* (tetragonal pyramidal), and 3*f* (octagonal), are in the primitive cell. One *m* site, two *o* sites, and two *h* sites are located on a plane of $(2\boldsymbol{a}+\boldsymbol{b},\boldsymbol{c})$ and four *n* sites, one *f* site, and two *i* sites are closely located on another plane of $(\boldsymbol{a},\boldsymbol{c})$. The hydrogen positions may change from these ideal ones because of the relaxation of atom positions after introduction of hydrogen. The determination of hydrogen positions is possible by neutron scattering (spectroscopy/diffraction)[8,9,11–17] and also by the first-principles calculations.[18–21]

In this study, the potential energy surfaces of the hydrogen atom on the two planes are at first obtained by the first-principles calculations, and then the possible hydrogen location regions are determined by considering the zero-point vibration energy. The hopping path between two sites is identified with the minimum energy path (MEP), which is determined by using the nudged elastic band (NEB) method.[22–24]

II. CALCULATIONS

First-principles calculations of the electronic structure were based on the density functional theory (DFT) using the projector augmented-wave (PAW) method[25] and the Perdew-Burke-Ernzerhof (PBE) version[26] of generalized gradient approximation (GGA) for the exchange-correlation potential. A program code, QMAS (Quantum MAterials Simulator) developed by Ishibashi *et al.*,[27] was employed. A primitive cell spanned by vectors ***a***, ***b***, and ***c*** was used as a unit cell under periodic boundary conditions in the calculation. A number of *k* points, 256 ($8\times8\times4$), and a cut-off energy for plane wave basis, 35 Ry, were employed. Although a higher cut-off energy and larger *k*-point numbers provide more accurate results, we chose the conditions providing a rather less but sufficiently accurate result, since numerous calculations are required to determine the potential energy surfaces and hopping paths of the hydrogen atom. Because of the same reason, the primitive cell is used as a unit cell in the DFT

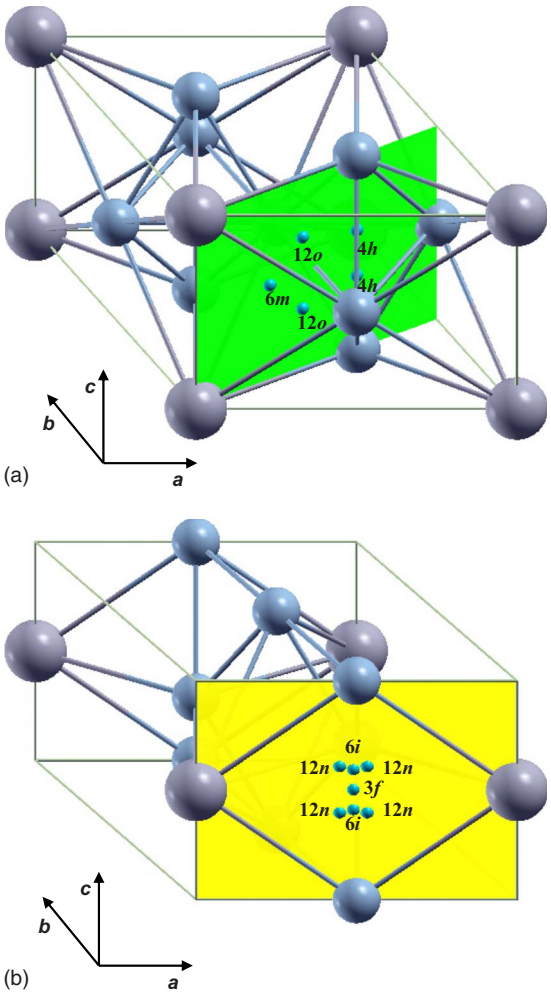

FIG. 1. (Color online) $LaNi_5$ unit cell and hydrogen sites. (a) *m*, *o*, and *h* sites on the plane spanned by vectors $2\boldsymbol{a}+\boldsymbol{b}$ and $\boldsymbol{c}$. (b) *n*, *f*, and *i* sites on the plane spanned by $\boldsymbol{a}$ and $\boldsymbol{c}$. Large balls are La atoms and middle balls are Ni atoms. Unit cell in (b) is shifted by $\boldsymbol{c}/2$ from that in (a).

calculation instead of the super cell. Lattice constants for $LaNi_5$ were obtained as $a=5.017$ Å and $c=3.943$ Å, where $a=\|\boldsymbol{a}\|$ and $c=\|\boldsymbol{c}\|$. These values are within the variation in the experimentally measured values, $a=5.011-5.032$ Å and $c=3.911-3.986$ Å.[3,4,12,13,15,17]

We considered a single hydrogen atom occupying a primitive cell, i.e., $LaNi_5H$. In this study, the total energy is converted to the hydrogen insertion energy, E_{ins}, defined by

$$E_{\mathrm{ins}} = E(\mathrm{LaNi_5H}) - [E(\mathrm{LaNi_5}) + (1/2)E(\mathrm{H_2})], \qquad (1)$$

where $E(\mathrm{LaNi_5H})$, $E(\mathrm{LaNi_5})$, and $E(\mathrm{H_2})$ are the total energies of the corresponding chemical composition in parentheses. $E(\mathrm{H_2})$ was calculated by placing a hydrogen molecule in the 10 Å $\times$ 10 Å $\times$ 10 Å cubic unit cell.

The hydrogen sites *m*, *o*, *h*, *n*, *i*, and *f* are shown in Fig. 1. All the atom positions in the unit cell are described as (x,y,z), where *x*, *y*, and *z* are fractional coordinates in terms of lattice vectors $\boldsymbol{a}$, $\boldsymbol{b}$, and $\boldsymbol{c}$, respectively. Three optimization levels were used: in level A, a hydrogen atom is simply inserted into a site of a $LaNi_5$ lattice without optimizing Ni atom positions (H position is optimized in the site energy calculations.), in level B, Ni atom positions are optimized by maintaining the lattice constants of $LaNi_5$, and in level C, in addition to level B, the lattice constants are also optimized by maintaining the hexagonal symmetry of the lattice.

When the cut-off energy was increased to 80 Ry, the total energy of $LaNi_5H$ decreased by 0.086 eV, and when the number of *k* points was increased to 2048 ($16\times16\times8$), the total energy increased by 0.020 eV for the *i* site in level C, for instance. Since we used the difference of the total energy under the different configurations as shown in Eq. (1), the values we used have higher accuracy; the insertion energy [Eq. (1)] changed only by 0.004 eV in the above case.

In NEB calculations,[22–24] we determined the MEP in levels A and B. The initial path was chosen as a straight line connecting the two hydrogen sites. Fifteen NEB nodes (hydrogen image atoms) were inserted along the path. Each neighboring node is connected with a spring and each node

TABLE I. Insertion energies E_{ins} in various optimized hydrogen site positions. Values of *x*, *y*, and *z* are fractional coordinates in terms of lattice vectors $\boldsymbol{a}$, $\boldsymbol{b}$, and $\boldsymbol{c}$, respectively.

		Level A			Level B			Level C				
		Position		E_{ins}	Position		E_{ins}	Position		Lattice constants (Å)		E_{ins}
Plane	Site	x,y	z	(eV)	x,y	z	(eV)	x,y	z	a	c	(eV)
$(2\boldsymbol{a}+\boldsymbol{b},\boldsymbol{c})$	$12o(2y,y,z)$	0.2085	0.2956	0.251	0.2208	0.3153	0.077	0.2240	0.3152	5.076	4.047	−0.017
	$6m(2y,y,1/2)$	0.1422	1/2	0.149	0.1529	1/2	0.105	0.1559	1/2	5.084	3.978	0.042
	$4h(2/3,1/3,z)$	2/3	0.3881	0.406	2/3	0.3831	0.127	2/3	0.3781	5.090	4.037	−0.014
$(\boldsymbol{a},\boldsymbol{c})$	$12n(x,0,z)$	0.4571	0.1060	0.189	[a]	[a]	[a]	[a]	[a]	[a]	[a]	[a]
	$6i(1/2,0,z)$	1/2	[a]	[a]	1/2	0.0868	−0.044	1/2	0.0916	5.058	4.015	−0.116
	$3f(1/2,0,0)$	1/2	0	0.326[b]	1/2	0	−0.002 [c]	1/2	0			

[a]Energy stationary point was not obtained.
[b]Energy local maximum.
[c]Saddle point.

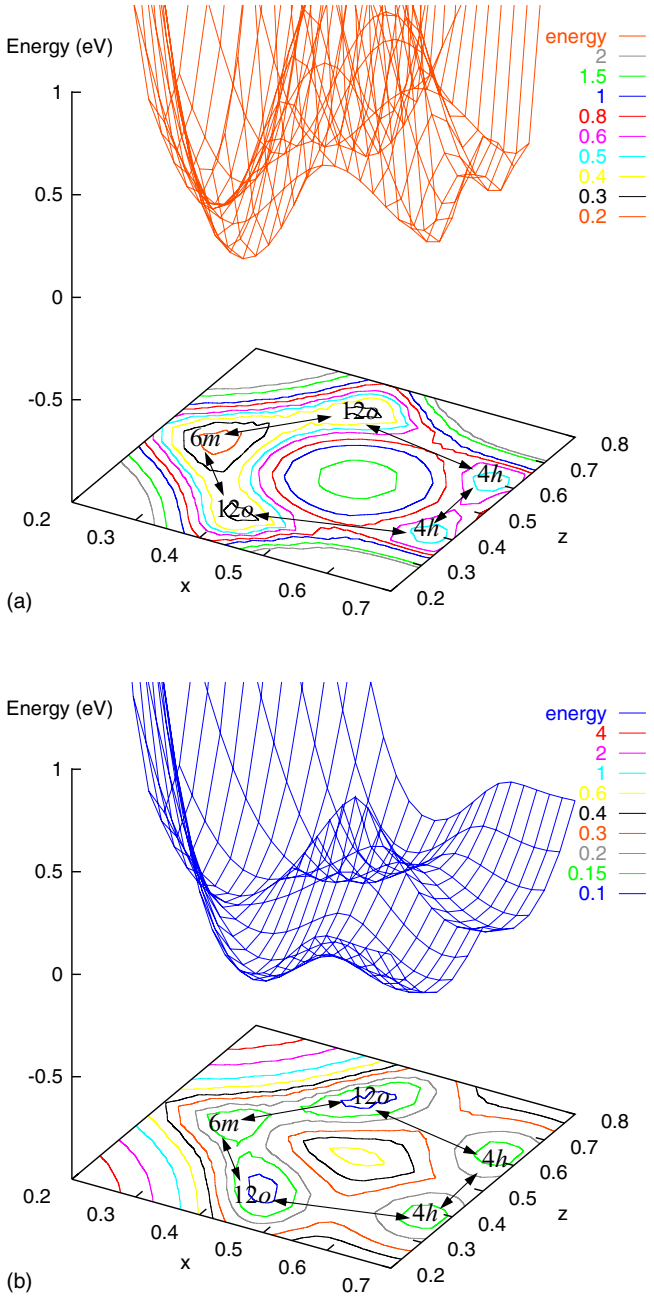

FIG. 2. (Color online) Hydrogen sites and potential energy surface of hydrogen on the plane spanned by vectors $2\boldsymbol{a}+\boldsymbol{b}$ and $\boldsymbol{c}$ in level A (a) and in level B (b). Hopping paths are shown by double headed arrows. Isolines for insertion energy E_{ins} are drawn at irregular intervals. Due to the mirror symmetry of the crystal, the calculations were performed for $z \leq 0.5$.

has the force from the spring and that obtained from the electronic structure calculation of the system.

III. RESULTS AND DISCUSSION

A. Hopping on the plane $(2\boldsymbol{a}+\boldsymbol{b},\boldsymbol{c})$

Optimized hydrogen positions on the plane spanned by $2\boldsymbol{a}+\boldsymbol{b}$ and $\boldsymbol{c}$ [see Fig. 1(a)] and the total energy obtained by the first-principles calculation with and without geometrical optimizations are given in Table I. When the optimization level is increased, the insertion energy at any site decreased. The hydrogen sites *o*, *m*, and *h* are on the plane and in the tetrahedra formed by La and Ni atoms.[29] Local displacements of Ni atoms are observed to increase the tetrahedral interstitial hole radius in level B and level C.[30] Although local displacements of La atoms are not observed because of a primitive cell used, such a displacements is implied in a super cell since in the level-C calculations the hole radius becomes greater than that in level B.

The potential energy surface of the hydrogen atom on the plane $(2\boldsymbol{a}+\boldsymbol{b},\boldsymbol{c})$ was obtained by the first-principles calculations by placing the hydrogen atom on each grid point at the interval of 0.01 for y and 0.05 for z.[28] The results are drawn with isoenergy lines in Fig. 2. Two geometrical optimization levels, A and B, were used in the total energy calculation. Three independent hopping paths of *m*-*o*, *o*-*h*, and *h*-*h* were found on this plane, as shown in Fig. 2. Each path intersects a triangle formed by three Ni/La atoms located on crossed planes with the $(2\boldsymbol{a}+\boldsymbol{b},\boldsymbol{c})$ plane. It is to be noted that there is no direct hopping path of *m*-*h* and *o*-*o*, both of which cross the Ni–Ni bond at, approximately, its center. Geometrical optimization in level B qualitatively gave the similar potential energy surface as that in level A; the precise site positions are changed and the insertion energies decrease.

Although it is possible to obtain the potential barriers between hydrogen sites from the potential energy surfaces shown in Fig. 2, the accuracy in the values is limited by the interval of grid points used to calculate the potential energy surface. In order to determine a more accurate energy barrier height and hopping path, the NEB method[22–24] was applied to determine the MEP between two energy local minimum sites. As expected from the mirror symmetry of the lattice, the MEPs obtained were on the plane $(2\boldsymbol{a}+\boldsymbol{b},\boldsymbol{c})$. The energy maximum point on the MEP is a saddle point in the potential energy surface. The energy barrier heights of various paths were calculated as the energy difference between a saddle point and a hydrogen site, as listed in Table II. The MEP of *h*-*h* is a straight line parallel to the lattice vector $\boldsymbol{c}$ due to the mirror symmetry, whereas the MEPs of others are curved. Local displacements of Ni atoms along the MEPs were also given in level B. The saddle point is on the common border triangle of two tetrahedra both of which contain the hydrogen sites. Ni atoms around the saddle points are displaced to enlarge the triangle.[30] The barrier heights are, therefore, decreased.

In the calculations described above, the quantum effect of hydrogen nucleus is not included, although the hydrogen atom, either ^{1}H or D, may behave as a quantum particle because of its small mass.[31] The potential barrier to be measured will be lower than the barriers listed in Table II due to the hydrogen zero-point vibration energy. We estimated the hydrogen zero-point vibration energy along the hopping path direction. The direction λ was determined by the tangent vector of the MEP at the hydrogen site. Displacing the hydrogen atom by $q=-0.20$ Å, -0.15 Å, -0.10 Å, …, 0.20 Å in the λ direction, hydrogen potential energy, $V_\lambda(q)$, were calculated. It was fitted to a parabolic curve as,

TABLE II. Barrier height of hydrogen hopping and zero-point vibration energy for ^{1}H and D in eV. In the barrier height, $X \rightarrow Y$ means the difference between the saddle point energy and the X site energy. In the zero-point vibration energy, $X \rightarrow Y$ means zero-point vibration energy at the X site along the direction of $X \rightarrow Y$ path.

			Barrier height				Zero-point vibration energy			
	Sites		Level A		Level B		^{1}H		D	
Plane	X	Y	$X \rightarrow Y$	$X \leftarrow Y$	$X \rightarrow Y$	$X \leftarrow Y$	$X \rightarrow Y$	$X \leftarrow Y$	$X \rightarrow Y$	$X \leftarrow Y$
$(2\boldsymbol{a}+\boldsymbol{b},\boldsymbol{c})$	m	o	0.188	0.086	0.049	0.076	0.06	0.07	0.04	0.05
	o	h	0.483	0.328	0.188	0.139	0.07	0.09	0.05	0.06
	h	h	0.203		0.127		0.09		0.06	
$(\boldsymbol{a},\boldsymbol{c})$	n	n	0.130 ($\boldsymbol{c}$ direction)		[a]		[a]		[a]	
			0.007 ($\boldsymbol{a}$ direction)		[a]		[a]		[a]	
	i	i	[a]		0.042		0.06		0.05	
Between planes	o	n	0.404	0.466	[a]	[a]	[a]	[a]	[a]	[a]
	o	i	[a]	[a]	0.247	0.369	0.08	0.06	0.06	0.04
	m	m	0.284		0.250		0.09		0.07	

[a]No path

$$V_\lambda(q) = (1/2)M\omega_\lambda^2 q^2 + V_0, \tag{2}$$

where M is the hydrogen atom mass, ω_λ is the angular frequency of the vibration to be fitted, and V_0 is the potential energy at the minimum. The vibration energy $E_\lambda^0 = (1/2)\hbar\omega_\lambda$ for each site and the direction of λ are included in Table II. Since the energy barrier in level B is 0.049 eV for $m \rightarrow o$, ^{1}H cannot be localized in a single site of m. The energy barrier for $o \rightarrow m$ is comparable to $E^0_{o\rightarrow m}$ for ^{1}H and that for $m \rightarrow o$ is comparable to $E^0_{m\rightarrow o}$ for D. With the help of thermal excitation at room temperature, both ^{1}H and D should spread over the adjacent o-m-o sites. We shall call this group of sites as the quasi-m site.

B. Hopping on the plane $(\boldsymbol{a},\boldsymbol{c})$

The hydrogen sites n, f, and i exist on the plane spanned by $\boldsymbol{a}$ and $\boldsymbol{c}$ [see Fig. 1(b)]. Optimized positions and the total energy for these sites were obtained in the same way as the case for the plane spanned by $2\boldsymbol{a}+\boldsymbol{b}$ and $\boldsymbol{c}$ (see Table I). The i site is the most stable as already pointed by Tatsumi *et al.*[19] and Zhang *et al.*[21] For the i site, both the H-Ni distance (1.63 Å in level B and 1.65 Å in level C) and the H-La distance (2.53 Å in level B and 2.56 Å in level C) are the longest among all hydrogen sites due to local and global displacements of Ni and La atoms.[30] The potential energy surface on the plane was obtained, as shown in Fig. 3, by placing a hydrogen atom on each grid point at the interval of 0.01 for x and z.

In the region of $-1/2 \leq z < 1/2$, four n sites with $(1/2 \pm 0.04, 0, \pm 0.11)$, one f site with (1/2, 0, 0), and two i sites with $(1/2, 0, \pm 0.09)$ (in level B) are located in a big octahedron surrounded by two La and four Ni atoms ($O[La_2Ni_4]$). From the lattice geometry consideration, n and f sites were proposed to be hydrogen sites.[29] On the plane $(\boldsymbol{a},\boldsymbol{c})$ the n site was a unique stable hydrogen position in the level A calculation, whereas the i site was a unique stable hydrogen position in levels B and C. It is to be noted that the f site is not a local minimum point in levels A, B, and C; it is at a local energy maximum in level A and a saddle point in level B (see Fig. 3). Although the energy values of the f site were reported in Refs. 19 and 21, it was not mentioned whether it was at a local minimum or not. Starting with the configuration of hydrogen placed at the f site with a small displacement, the hydrogen atom moved toward the n site (level A) or the i site (levels B and C).

There are two kinds of paths between four n sites; one is between the sites with $(1/2 \pm 0.04, 0, z)$ and another is between the sites with $(x, 0, \pm 0.11)$, as shown in Fig. 3(a). The NEB calculation in level A provided a very small energy barrier (0.007 eV) for the former path and a large energy barrier (0.13 eV) for the latter path (see Table II). For the path of i-f-i in level B, the energy barrier height was calculated to be 0.042 eV, the saddle point being at the f site. Since $E^0_{i\rightarrow i}$ was estimated to be 0.06 eV for ^{1}H and 0.05 eV for D (see Table II) at the i site, both ^{1}H and D are not localized on the i site but are distributed between two i sites. We call this i-f-i region as a quasi-f site. This quasi-f site is the most stable even after considering the zero-point vibration energy.

The hydrogen site position in the solid solution phase can be directly determined by the neutron diffraction experiment. Fischer *et al.*[11] showed that the f site is occupied. Soubeyroux *et al.*[13] compared the f site and the n site models in Rietveld refinement and concluded that the n site model is more probable than the other. Kisi *et al.*[15] showed that starting Rietveld refinement from the n site with (0.45, 0, 0.11), the x coordinate always converged toward 1/2, i.e., the i site, and oscillated. Although the i sites with $(1/2, 0, \pm 0.09)$ is the energy minimum in the level B calculation, we concluded the quasi-f site to be the most probable "occupation site." Hydrogen atom at the n site will move to the quasi-f site.

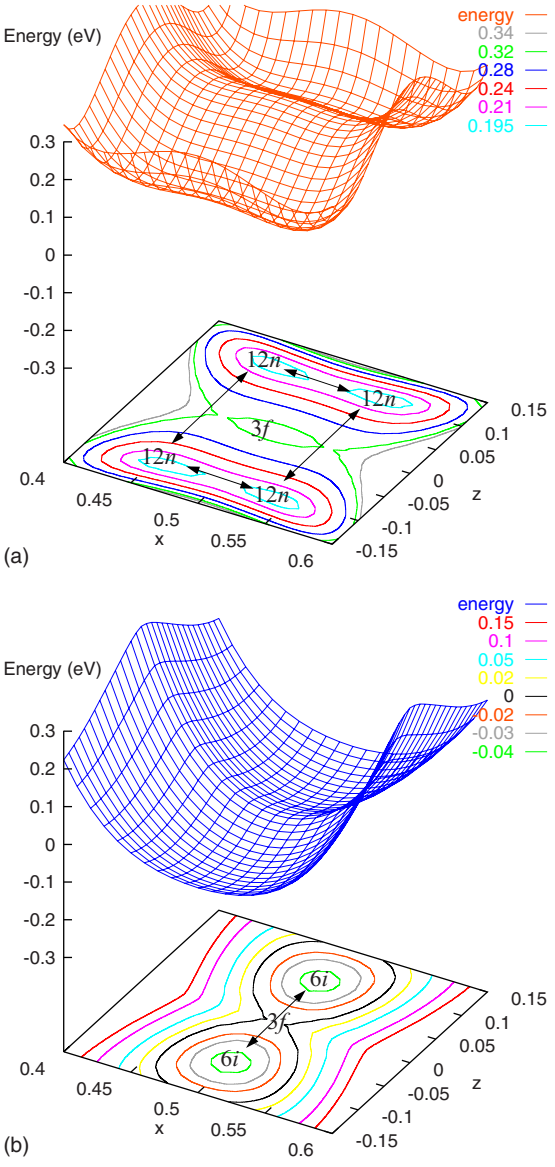

FIG. 3. (Color online) Hydrogen sites and potential energy surface on the plane spanned by vectors $\boldsymbol{a}$ and $\boldsymbol{c}$ in level A (a) and in level B (b). Hopping paths are shown by double headed arrows. Isolines for insertion energy E_{ins} are drawn at irregular intervals. Due to the mirror symmetry of the crystal, the calculations were performed for $x \leq 0.5$ and $z > 0$.

C. Other hopping paths

There is a hopping path o-i connecting the two planes $(2\boldsymbol{a}+\boldsymbol{b},\boldsymbol{c})$ and $(\boldsymbol{a},\boldsymbol{c})$. It is one of the important paths because it connects the i site, which is in the most probable occupation site, and quasi-f. This path and another hopping path m-m on a plane spanned by $\boldsymbol{a}$ and $\boldsymbol{b}$ were calculated via the NEB method both in level A and level B. The former path is curved and does not lie on any plane.[28] The energy barrier heights of these paths are included in Table II. In level B, the $i \rightarrow o$ hopping has the largest barrier height, followed by the $o \rightarrow i$ and m-m hoppings.

Even though another candidate of the hopping path, e.g., the direct connection between the n and h sites, can be considered, the path has a high energy barrier, since such a path cuts across the Ni-Ni bond. In fact, when we performed the NEB calculation of the n-h path in level A, no direct MEP of n-h hopping was found. Instead, the path converged to the MEP which consists of successive hopping of n-o and o-h.

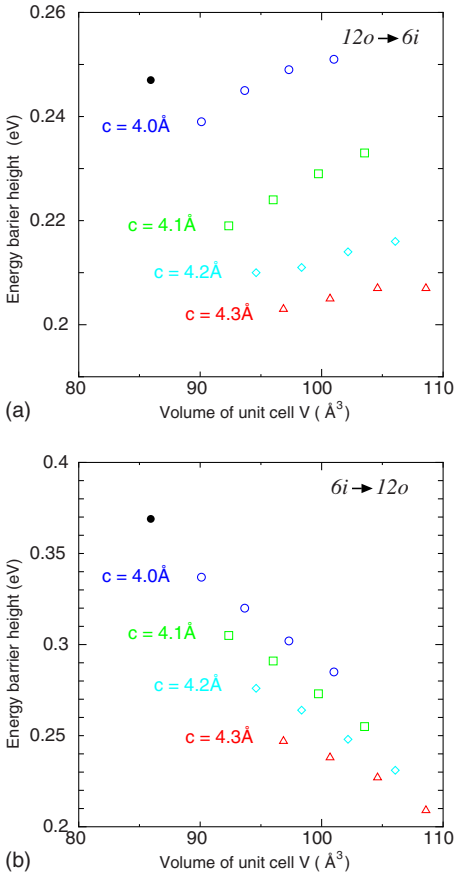

FIG. 4. (Color online) Energy barrier height of $o \rightarrow i$ hopping (a) and of $i \rightarrow o$ hopping (b) at various lattice constants as a function of the lattice volume. The barrier height for $a=5.017$ Å and $c=3.943$ Å is shown by a solid circle.

D. Effect of lattice expansion

We did not calculate the barrier heights in level C, which includes the lattice optimization, although the barrier heights might be affected by the lattice parameter. In order to observe this effect, we performed a NEB calculation for the i-o path in level B under the conditions that lattice constants are "pre-expanded" before the NEB calculation. The lattice constants were set in the region of $a=5.10-5.40$ Å and $c=4.0-4.3$ Å, which were chosen to be between the lattice constant of solid solution $LaNi_5H$ and that of hydride $LaNi_5H_6$.[3,4,15,17] The barrier height of $o \rightarrow i$ hopping decreased as c increased, as shown in Fig. 4. It increased only a little as a increased. The barrier height of $i \rightarrow o$ hopping decreased as a and c increased. When c is expanded to 4.3 Å, which corresponds to that of the hydride, the barrier height of $i \rightarrow o$ hopping decreased from 0.369eV to 0.235eV. When comparable expansion actually occurs in the solid solution phase surrounded by hydride $LaNi_5H_6$, hydrogen dif-

fusion in the solid solution region will be accelerated.

The saddle point energy in the *i*-*o* path was the lowest (0.222 eV) at a=5.10 Å and c=4.0 Å in the lattice expansion calculations. The difference between this lowest saddle point energy (0.222eV) and the *i* or *o* site energy in level C is corresponding to the barrier height energy in the level C calculation. The estimated barrier heights are 0.239 eV for $o \rightarrow i$ hopping and 0.338 eV for $i \rightarrow o$ hopping, smaller than level B by 0.008 eV (for $o \rightarrow i$) and 0.031 eV (for $i \rightarrow o$). Although the barrier height energy is decreased by the lattice expansion, it is not obvious that the lattice expansion effectively takes place in the real system when the hydrogen diffuses. It is necessary to take into account an entropy term in the saddle point *free energy*. In order to include the entropy effect in the simulation, the first principles molecular dynamics (with e.g., blue-moon ensemble method) is needed; such a simulation is impossible at the moment, however.

E. Diffusion route and activation energy

Diffusion is observed as a result of successive hopping through various paths. Several diffusion routes are possible, as illustrated in Fig. 5. For the diffusion in the ***c***-direction, a route of quasi-*f* (1/2, 0, 0)–quasi-*m* $(x,x/2,1/2)$–quasi-*f* (1/2, 0, 1) and some equivalent routs are possible. The energy difference between the highest saddle point energy (in *o*-*i*) and the lowest site energy (at *i*) in the route, 0.369 eV, will be approximately the activation energy in the ***c***-direction diffusion, although quantum effects such as zero-point vibration energy at hydrogen sites, the quantization of the activated state, and the tunnel effect must be considered[31] to quantitatively compare it with the experiments. Diffusion route through the *h* site does not contribute to the diffusion, since the *o*-*h* and *h*-*h* paths have the larger barrier height than that in *m*-*o*. Well-coincident activation energy, 0.367eV, was reported by Ziichner *et al.*,[5] who measured it by using the Arrhenius plot of diffusion coefficient along the ***c*** direction in the $LaNi_5$ single crystal.

For the diffusion in the ***a***-direction, several inequivalent routes are possible, as shown in Fig. 5(b). Route A [quasi-*f* (0, 1/2, 0)–quasi-*m*–quasi-*f*–quasi-*m*–quasi-*f* (1, 1/2, 0)] has the highest saddle point in *i*-*o*. Another routes such as B (quasi-*f*–quasi-*m*–quasi-*m*–*h*–quasi-*m*–quasi-*f*), C (quasi-*f*–quasi-*m*–quasi-*m*–quasi-*f*–quasi-*m*–quasi-*f*), and D [quasi-*m* $(-y,y,1/2)$–quasi-*m*–quasi-*m*–*h*–quasi-*m* $(1-y,y,1/2)$] have the highest saddle point in *m*-*m*. Activation energies estimated from these saddle point energies are 0.369 eV (route A) and 0.399 eV (routes B, C, and D). Although the lower activation energy should be observed at low temperature limit, the higher activation energy might be observed at some temperature region. In either case, small anisotropy in the activation energy is expected. Our estimation is supported from the measured activation energy reported in Ref. 5, 0.395 eV, in the ***a***-direction diffusion and that in polycrystalline $LaNi_5$,[6,7] 0.3 eV–0.5 eV.

IV. CONCLUSION

The potential energy surface for hydrogen, the minimum energy path, and the barrier height of hydrogen hopping for all possible paths were obtained by using the first-principles electronic structure calculations. Hydrogen sites were grouped to quasi-*m* site (*o*-*m*-*o* sites), *h* site, and quasi-*f* site (*i*-*f*-*i* sites) by taking into account the zero-point vibration energy along the hopping directions after all atom optimizations. The activation energy estimated from the saddle point energy in the ***a***- and ***c***-directions is 0.37 eV, which is in good agreement with the experimental values, 0.3–0.5 eV.

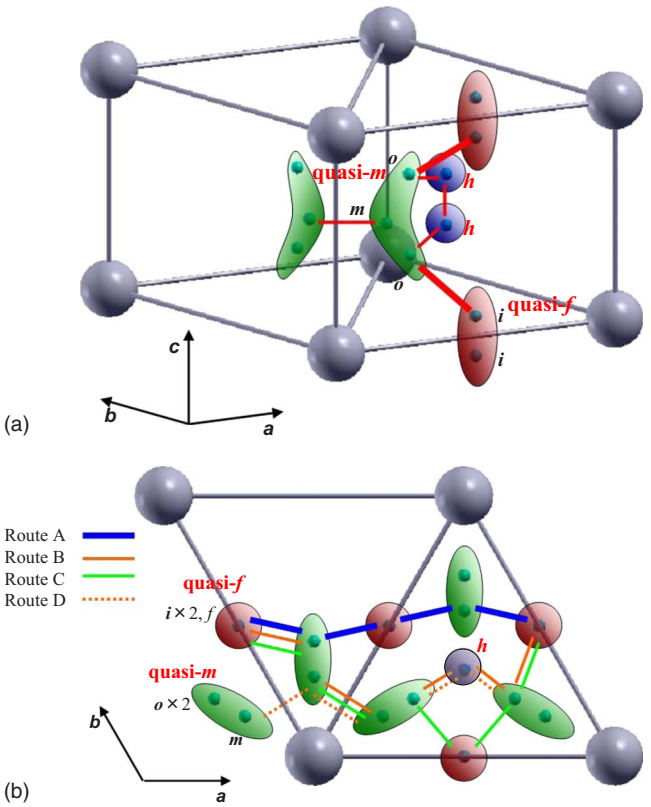

FIG. 5. (Color online) Diffusion routes in the ***a*** and ***c*** directions. Only La atoms are shown by large balls. Some hydrogen sites are grouped to the quasisites. (a) The diffusion route in the ***c*** direction (thick red lines). Hopping paths shown by thin red lines do not contribute to the diffusion. (b) Top view of the diffusion routes in the ***a*** direction. Four representative routes, A, B, C, and D, are shown by different colors.

ACKNOWLEDGMENTS

This work is supported by New Energy and Industrial Technology Development Organization (NEDO) under "Advanced Fundamental Research Project on Hydrogen Storage Materials." First-principles calculations were performed on AIST Super Cluster. One of the authors (A.T.) would like to thank N. Orita for his help on using QMAS. He also would like to thank T. Kaneko for his discussion. For Figs. 1 and 5, XCrySDen (Ref. 32) was used.

*tezuka.akinori@aist.go.jp
†Present address: International Research Center for Nuclear Materials Science, Institute for Materials Research, Tohoku University, Narita-cho 2145-2, Oarai-machi, Ibaraki 311-1313, Japan.
‡Present address: New Industry Creation Hatchery Center (NICHe), Tohoku University, 6-6-10 Aoba, Aramaki, Aoba-ku, Sendai 980-8579, Japan.

[1] J. H. N. van Vucht, F. A. Kuijpers, and H. C. A. M. Bruning, Philips Res. Rep. **25**, 133 (1970).
[2] J. J. G. Willems and K. H. J. Buschow, J. Less-Common Met. **129**, 13 (1987).
[3] S. Ono, K. Nomura, E. Akiba, and H. Uruno, J. Less-Common Met. **113**, 113 (1985).
[4] E. Akiba, K. Nomura, and S. Ono, J. Less-Common Met. **129**, 159 (1987).
[5] H. Züchner, T. Rauf, and R. Hempelmann, J. Less-Common Met. **172-174**, 611 (1991).
[6] T. Haraki, N. Inomata, and H. Uchida, J. Alloys Compd. **293-295**, 407 (1999).
[7] K. Asano, Y. Hashimoto, T. Iida, M. Kondo, and Y. Iijima, J. Alloys Compd. **395**, 201 (2005).
[8] D. Richter, R. Hempelmann, and C. Schönfeld, J. Less-Common Met. **172-174**, 595 (1991).
[9] C. Schönfeld, R. Hempelmann, D. Richter, T. Springer, A. J. Dianoux, J. J. Rush, T. J. Udovic, and S. M. Bennington, Phys. Rev. B **50**, 853 (1994).
[10] J. L. C. Daams, P. Villars, and J. H. N. van Vucht, *Atlas of Crystal Structure Types for Intermetallics Phases* (ASM International, Ohio, 1991).
[11] A. Fischer, A. Furrer, G. Busch, and L. Schlapbach, Helv. Phys. Acta **50**, 421 (1977).
[12] R. Hempelmann, D. Richter, G. Eckold, J. J. Rush, J. M. Rowe, and M. Montoya, J. Less-Common Met. **104**, 1 (1984).
[13] J. L. Soubeyroux, A. Percheron-Guegan, and J. C. Achard, J. Less-Common Met. **129**, 181 (1987).
[14] H. Hayakawa, K. Nomura, Y. Ishido, E. Akiba, and S. Shin, J. Less-Common Met. **143**, 315 (1988).
[15] E. H. Kisi, E. M. A. Gray, and S. J. Kennedy, J. Alloys Compd. **216**, 123 (1994).
[16] E. M. A. Gray, M. Kemali, J. Mayers, and J. Norland, J. Alloys Compd. **253-254**, 291 (1997).
[17] M. P. Pitt, E. M. A. Gray, E. H. Kisi, and B. A. Hunter, J. Alloys Compd. **293-295**, 118 (1999).
[18] H. Nakamura, D. Nguyen-Manh, and D. G. Pettifor, J. Alloys Compd. **281**, 81 (1998).
[19] K. Tatsumi, I. Tanaka, H. Inui, K. Tanaka, M. Yamaguchi, and H. Adachi, Phys. Rev. B **64**, 184105 (2001).
[20] L. G. Hector, Jr., J. F. Herbst, and T. W. Capehart, J. Alloys Compd. **353**, 74 (2003).
[21] C. Zhang, T. Gao, X. Qi, Y. Zhang, L. Tang, J. Zhou, and B. Chen, Physica B **403**, 2372 (2008).
[22] G. Mills and H. Jónsson, Phys. Rev. Lett. **72**, 1124 (1994).
[23] G. Henkelman, B. P. Uberuaga, and H. Jónsson, J. Chem. Phys. **113**, 9901 (2000).
[24] G. Henkelman and H. Jónsson, J. Chem. Phys. **113**, 9978 (2000).
[25] P. E. Blöchl, Phys. Rev. B **50**, 17953 (1994).
[26] J. P. Perdew, K. Burke, and M. Ernzerhof, Phys. Rev. Lett. **77**, 3865 (1996).
[27] S. Ishibashi, K. Terakura, and H. Hosono, J. Phys. Soc. Jpn. **77**, 053709 (2008).
[28] A. Tezuka, H. Wang, H. Ogawa, and T. Ikeshoji, Int. J. Nanosci. **8**, 49 (2009).
[29] D. G. Westlake, J. Less-Common Met. **91**, 275 (1983).
[30] See supplementary material at http://link.aps.org/supplemental/10.1103/PhysRevB.81.134304 for the displacement of Ni atoms and the interstitial hole radii.
[31] Y. Fukai and H. Sugimoto, Adv. Phys. **34**, 263 (1985).
[32] A. Kokalj, J. Mol. Graphics Modell. **17**, 176 (1999). Code available from http://www.xcrysden.org/